Bifurcation in a nonlinear autoparametric system using experimental and numerical investigations

Alain Berlioz, Régis Dufour, Subhash Sinha

Bifurcation in a Nonlinear Autoparametric System Using Experimental and Numerical Investigations

A. BERLIOZ and R. DUFOUR
Laboratoire de Mécanique des Structures, UPRESA CNRS 5006, INSA de Lyon, 69621 Villeurbanne, France

S. C. SINHA
Nonlinear Systems Research Laboratory, Department of Mechanical Engineering, Auburn University, Auburn, AL 36849, U.S.A.

Abstract. Experimental and numerical investigations are carried out on an autoparametric system consisting of a composite pendulum attached to a harmonically base excited mass-spring subsystem. The dynamic behavior of such a mechanical system is governed by a set of coupled nonlinear equations with periodic parameters. Particular attention is paid to the dynamic behavior of the pendulum. The periodic doubling bifurcation of the pendulum is determined from the semi-trivial solution of the linearized equations using two methods: a trigonometric approximation of the solution and a symbolic computation of the Floquet transition matrix based on Chebyshev polynominal expansions. The set of nonlinear differential equations is also integrated with respect to time using a finite difference scheme and the motion of the pendulum is analyzed via phase-plane portraits and Poincaré maps. The predicted results are experimentally validated through an experimental set-up equipped with an opto-electronic set sensor that is used to measure the angular displacement of the pendulum. Period doubling and chaotic motions are observed.

Keywords: Dynamic instability, autoparametric system, experiment, chaotic motion, nonlinear motion, symbolic computational technique, Chebyshev polynomials.

1. Introduction

Autoparametric systems consist of parametrically excited subsystems nonlinearly coupled to externally excited subsystems [1]. Many authors have studied this type of system, which displays various phenomena and, under particular conditions, may offer an unintuitive dynamic behavior (see, for example, [2–4]). The phenomena, common to several scientific domains (chemistry, electronics, electromechanical, etc.), reveal a universal nature and, for that reason, are interesting to investigate [5].

The main aim of the present study is to make an experimental contribution to the analysis of autoparametric mechanical systems. In the present case, the system consists of a compound pendulum hinged to a mass-spring subsystem that is harmonically based-excited. A similar problem has been theoretically investigated in [6, 7] where the mass-spring subsystem is force-excited.

The following section describes the set of coupled nonlinear equations governing the physical problem. The stability and bifurcation of the semi-trivial solution, which corresponds to the bottom equilibrium position of the pendulum [8], is investigated by two methods. In the first approach, the solution is approximated by a two-term trigonometric function and the method of harmonic balance is applied. The second method uses a shifted Chebyshev

Figure 1. Schematic of the experimental set-up.

polynomials expansion of the time-periodic state matrix and Picard's iteration technique to obtain the Floquet transition matrix in a symbolic form [9], which can be used to predict the primary bifurcation of period doubling. The time response of the solutions of the set of nonlinear equations is also obtained by using the Runge–Kutta method contained in the MATLAB software package. In Section 3, the experimental set-up is described and measurement procedures are provided. A comparison of numerical and experimental results is presented in Section 4. Attention is paid to the bifurcation diagram and to the time response of the system that, under certain conditions, exhibits chaotic behavior [10].

2. Equations of Motion and Numerical Investigations

2.1. EQUATIONS

Let the parametrically excited subsystem be a compound pendulum hinged at point O and let m, L and I_o be its mass, length and moment of inertia with respect to O, respectively. Furthermore, let the externally excited subsystem be composed of a mass M that is assumed to move vertically and a linear spring k (Figure 1). The two degrees of freedom of the system are the vertical displacement of the mass along z, and θ the angular position of the pendulum. Let c and c_1 be the damping coefficients of the vertical and angular motions, respectively. The base of the spring has a vertical harmonic displacement of amplitude a and frequency ω. The

equations, which govern the dynamic behavior of the system with a simple pendulum, are well known (see, for example, [11]). In the case of a compound pendulum, the equations become similar and can be written as

$$(M+m)\ddot{z} + c\dot{z} + kz + ml(\ddot{\theta}\sin\theta + \dot{\theta}^2\cos\theta) = (M+m)a\omega^2\cos\omega t,$$
$$m\rho^2\ddot{\theta} + c_1\dot{\theta} + mgl\sin\theta + ml(\ddot{z} - a\omega^2\cos\omega t)\sin\theta = 0, \tag{1}$$

where the dot denotes a derivative with respect to time t and l is the location of the center of mass with respect to O. The radius of gyration $\rho = (I_0/m)^{1/2}$. It is convenient to use a nondimensional form in which the prime denotes the derivatives with respect to τ, the new dimensionless time variable

$$w'' + Kw' + q^2 w + \gamma(\theta''\sin\theta + \theta'^2\cos\theta) = \varepsilon\eta^2\cos\eta\tau,$$
$$\theta'' + K_1\theta' + \sin\theta + (w'' - \varepsilon\eta^2\cos\eta\tau)\sin\theta = 0, \tag{2}$$

with

$$\tau = \omega_1 t, \quad w = \frac{zl}{\rho^2}, \quad \varepsilon = \frac{al}{\rho^2},$$
$$\gamma = \frac{ml^2}{(M+m)\rho^2}, \quad \eta = \frac{\omega}{\omega_1}, \quad q = \frac{\omega_0}{\omega_1},$$
$$\omega_0 = \sqrt{\frac{k}{M+m}}, \quad \omega_1 = \sqrt{\frac{gl}{\rho^2}}, \tag{3}$$

where ω_0 is the natural frequency of the externally excited subsystem and ω_1 the natural frequency of the parametrically excited subsystem.

2.2. Stability and Bifurcation Diagrams

This consists in establishing the equation of the stability boundary curve in the plane (ε, η) of the pendulum. Particular attention is paid to the primary bifurcation where the pendulum has a period-doubling motion.

For $\theta_o = 0$ equilibrium position, Equations (2) reduce to

$$w_0'' + Kw_0' + q^2 w_0 = \varepsilon\eta^2\cos\eta\tau, \tag{4}$$

whose semi-trivial solution is:

$$w_0(\tau) = \varepsilon(A\cos\eta\tau + B\sin\eta\tau),$$
$$\theta_0(\tau) = 0. \tag{5}$$

Substituting Equation (5) into (4) yields

$$A = \frac{\eta^2(q^2-\eta^2)}{(q^2-\eta^2)^2 + (K\eta)^2}, \quad B = \frac{K\eta^3}{(q^2-\eta^2)^2 + (K\eta)^2}. \tag{6}$$

The stability of the semi-trivial solution is investigated by introducing small perturbation u and φ, as

$$w = w_0 + u, \quad \theta = \theta_0 + \varphi. \tag{7}$$

Retaining only the linear terms, Equation (2) yields

$$u'' + Ku' + q^2 u = 0, \tag{8}$$

$$\varphi'' + K_1\varphi' + \varphi - \varepsilon\eta^2[(1 + A)\cos\eta\tau + B\sin\eta\tau] = 0. \tag{9}$$

2.2.1. *Harmonic Approximation*

Equation (8) has an exponentially decaying solution while the stability of the Mathieu Equation (9) depends on the parameters ε and η. As a first-order approximation, its solution may be assumed as

$$\varphi = C\cos\frac{1}{2}\eta\tau + D\sin\frac{1}{2}\eta\tau. \tag{10}$$

Substituting Equation (10) into (9) and equating the sine and cosine terms leads to a set of two algebraic equations. Seeking a nontrivial solution, the determinant is set to zero to find the stability boundary (or bifurcation curve) of the pendulum as a function of η:

$$\varepsilon = \frac{2}{\eta^2}\sqrt{\frac{\left(1 - \frac{1}{4}\eta^2\right)^2 + \frac{1}{4}K_1^2\eta^2}{(1 + A)^2 + B^2}}. \tag{11}$$

It should be noted that in the classical case, where the hinge point O has a harmonic displacement, Equation (11) reduces to

$$\varepsilon = \frac{2}{\eta^2}\sqrt{\left(1 - \frac{1}{4}\eta^2\right)^2 + \frac{1}{4}K_1^2\eta^2}. \tag{12}$$

2.2.2. *Symbolic Computation of the Floquet Transition Matrix*

Equation (9) can be rewritten in the state-space form as

$$\begin{Bmatrix} \phi_1' \\ \phi_2' \end{Bmatrix} = \begin{bmatrix} 0 & 1 \\ 1 + \varepsilon\eta^2[(1 + A)]\cos\eta\tau + \sin\eta\tau & -K_1 \end{bmatrix} \begin{Bmatrix} \phi_1 \\ \phi_2 \end{Bmatrix}, \tag{13}$$

where $\phi_1 = \phi$ and $\phi_2 = \phi'$.

The Floquet transition matrix associated with Equation (13) can be computed symbolically following the approach suggested by Sinha and Butcher [9]. Then the local stability and bifurcation conditions can be obtained in terms of system parameters as shown in [12]. Consider a general linear system

$$\dot{\mathbf{x}} = \mathbf{A}(t, \alpha), \quad \mathbf{x}(\mathbf{0}) = \mathbf{x}^0, \tag{14}$$

where α is the set of system parameters and $\mathbf{A}(t, \alpha)$ is a periodic matrix with period $t = KT$; $K = 1, 2, \ldots$. Equation (14) can be expressed in the integral form

$$\mathbf{x}(t) = \mathbf{x}^0 + \int_0^t \mathbf{A}(\tau, \alpha)\mathbf{x}(\tau)\,\mathrm{d}\tau, \tag{15}$$

and by employing Picard iteration to find the $(K+1)$th approximation

$$\begin{aligned}\mathbf{x}^{(k+1)}(t) &= \mathbf{x}^0 + \int_0^t \mathbf{A}(\tau_k,\alpha)\mathbf{x}^{(k)}(\tau_k)\,\mathrm{d}\tau_k \\ &= \left[\mathbf{I} + \int_0^t \mathbf{A}(\tau_k,\alpha)\,\mathrm{d}\tau_k + \int_0^t \mathbf{A}(\tau_k,\alpha)\int_0^{\tau_k}\mathbf{A}(\tau_{k-1},\alpha)\,\mathrm{d}\tau_{k-1}\,\mathrm{d}\tau_k \right. \\ &\quad \left. + \cdots + \int_0^t \mathbf{A}(\tau_k,\alpha)\ldots\int_0^{\tau_1}\mathbf{A}(\tau_0,\alpha)\,\mathrm{d}\tau_0\ldots\mathrm{d}\tau_k\right]\mathbf{x}^0, \end{aligned} \tag{16}$$

where $\tau_0, \tau_1, \ldots, \tau_k$, are all dummy variables and $\mathbf{I}$ the identity matrix. The expression in brackets is an approximation to the fundamental solution matrix since it is truncated after a finite number of terms (iterations). After the period is normalized to 1 via the transformation $t = KT\tau$, the normalized 1-periodic system matrix $\bar{\mathbf{A}}(\tau,\alpha) = \bar{\mathbf{A}}(\tau+1,\alpha)$ is expanded in m-shifted Chebyshev polynomials of the first kind valid in the interval [0, 1] as

$$\bar{\mathbf{A}}(\tau,\alpha) = \hat{\mathbf{T}}^T(\tau)\mathbf{D}(\alpha), \tag{17}$$

where $\hat{\mathbf{T}}^T(\tau)$ is the $N \times Nm$ Chebyshev polynomial matrix and $\mathbf{D}(\alpha)$ is the $Nm \times N$ Chebyshev coefficient matrix. When this is inserted into Equation (16), the integration and product operational matrices associated with the Chebyshev polynomials may be employed to achieve an expression for the expansion of $\mathbf{\Phi}(\tau,\alpha)$ in shifted Chebyshev polynomials as

$$\mathbf{\Phi}^{(p,m)}(\tau,\alpha) = \hat{\mathbf{T}}^T(\tau) + \left[\hat{\mathbf{I}} + \left(\sum_{k=1}^{p}[\mathbf{L}(\alpha)]^{k-1}\right)\mathbf{P}(\alpha)\right] = \mathbf{T}^T(\tau)\mathbf{B}(\alpha), \tag{18}$$

where the $Nm \times N$ Chebyshev coefficient matrix $\mathbf{B}(\alpha)$ is expressed in terms of $\mathbf{I}$, $\mathbf{L}(\alpha) = \hat{\mathbf{G}}^T\hat{\mathbf{Q}}_D(\alpha)$ and $\mathbf{P}(\alpha) = \hat{\mathbf{G}}^T\mathbf{D}(\alpha)$. Additional details on this algorithm, including the operational matrices $\hat{\mathbf{I}}$, $\hat{\mathbf{G}}$ and $\hat{\mathbf{Q}}_D$ and the 'alternate formulation', are given in [9]. By selecting the number p of Picard iterations and the number m of polynomials, this truncated expression yields an approximate expression for $\mathbf{\Phi}(kT,\alpha)$ to any desired accuracy. Conditions for various codimension 1 bifurcations are stated in [12]. In this particular case, the system undergoes a flip bifurcation which implies that one of the Floquet multipliers is -1 and

$$\det(\mathbf{I} + \mathbf{H}(\alpha)) = 0, \quad \mathbf{H}(\alpha) = \mathbf{\Phi}(2kT,\alpha). \tag{19}$$

2.2.3. *Simulation of Nonlinear Equations*

Nonlinear equations (1) are written in the state-space form. For a given set of four initial conditions, the time integration is performed using the Runge–Kutta scheme with a 0.001 s time step. The time history is plotted in the phase-plane and/or as Poincaré portraits. The Simulink Toolbox (a part of MATLAB software) is used for convenience in computing these solutions.

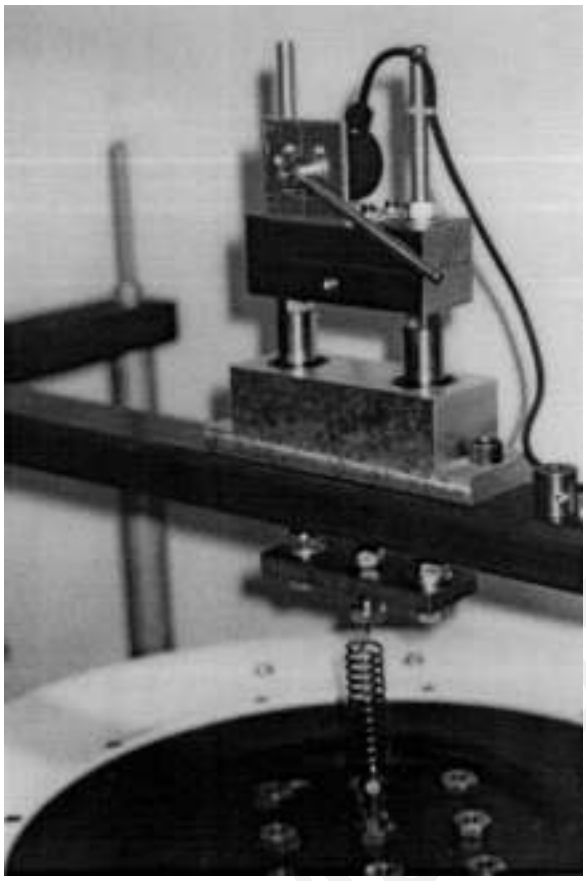

Figure 2. Experimental set-up.

3. Experimental Investigation

3.1. Experimental Set-Up

The experimental set-up is shown in Figure 2. The mass M is guided vertically by two slide bearings having a small friction coefficient. The mass is connected to the head of an electro-dynamic shaker with a linear spring of modulus k. The 4670 N Gearing & Watson shaker is used to provide the sinusoidal input and is designed to have a 51 mm peak-to-peak maximum displacement. The compound pendulum, which consists of a circular cross-section rod, is hinged to the axis of the opto-electronic sensor, which is used to measure the angular displacement. Measurements of the vertical excitation amplitude are obtained using an integrated circuit piezoelectric accelerometer screwed on the shaker head (the base), while the vertical motion of the mass is measured with an identical accelerometer stuck onto the sliding mass (see the schematic presented in Figure 1).

The incremental digital sensor (which has no angular limitation) produces 3600 pulses per revolution. It is able to detect a change in direction of rotation through a counter card plugged into a PC. A specific computer program in Pascal language is developed in order to obtain and store the time history of the angular position of the pendulum, from which instantaneous

Table 1. Values of the device parameters.

Parameters	Values
M	2.400 kg
m	0.030 kg
l	0.033 m
ρ	0.046 m
k	2700 N/m
ω_0	33.3 rad/s
ω_1	12.3 rad/s
α_0	1.8×10^{-4}
α_1	1.0×10^{-4}
c	2.9 Ns/m
c_1	1.6×10^{-5} Nms
q	2.72
K	0.10
K_1	0.02

speed of rotation is deduced. Several time cycles have been tried and it appears that 8192 μs is sufficient. The results are analyzed with computer programs in MATLAB language.

3.2. Experimental Procedure

Modal parameters of the dynamic system are measured and recorded in Table 1, with preliminary experimental investigations. The natural frequency ω_0 and the viscous damping factor α_0 are determined from sine wave transmissibility response and free oscillations of the mass-spring subsystem. The natural frequency ω_1 and the viscous damping factor α_1 of the pendulum are, in turn, measured with small free oscillations. The l dimension is measured and inertia I_0 deduced from ω_1. The damping coefficients c and c_0 of the two subsystems are calculated according to the relationships:

$$c = 2\alpha_0\sqrt{k(M+m)}, \quad c_1 = 2\alpha_1\sqrt{I_0 mgl}. \tag{20}$$

The instability threshold of the pendulum is investigated by changing the amplitude a and keeping the forcing frequency ω constant. When the mass-spring subsystem achieves a steady-state oscillating motion, spectral analysis is performed on the accelerometer signals. Thus, the rms acceleration levels of the mass and of the base are recorded and converted into a displacement level. Then a small angular deviation (around 6°) is applied to the pendulum. The asymptotic stability is registered when the pendulum returns to its static equilibrium position. The forcing frequency ω is increased from 3.0 to 6.3 Hz in 0.1 Hz increments. A bifurcation diagram is plotted at the 3.5 Hz fixed forcing frequency, which is close to the middle of the interval $[\omega_1, \omega_0]$. Manual sweeps (up and down) are performed on the displacement amplitude of the base from 0.3 to 5.7 mm. At the same time, the motion of the pendulum is analyzed with phase-plane portraits and Poincaré maps sampled at the time period of the excitation.

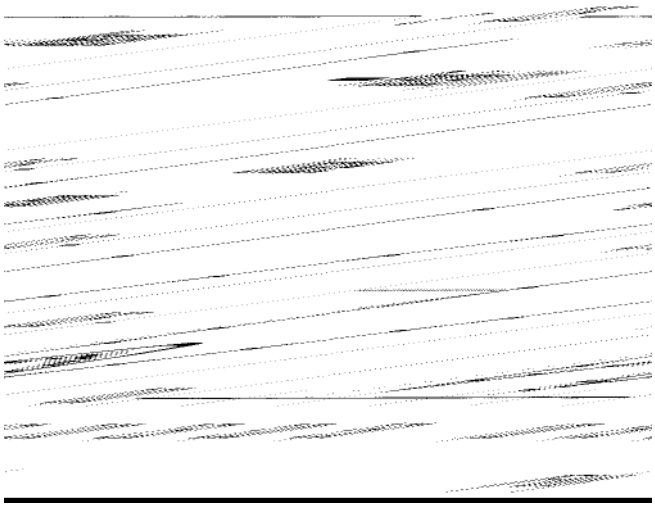

Figure 3. Stability boundary of the pendulum in the ε–η plane.

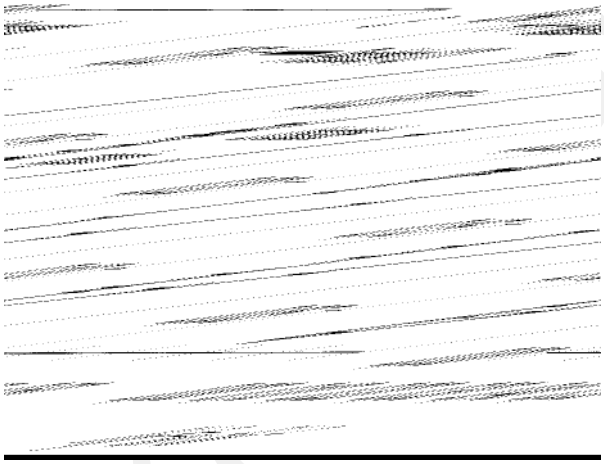

Figure 4. Stability boundary of the pendulum in the ε–η^{-2} plane.

4. Comparison of Numerical and Experimental Results

4.1. Stability Boundary

In Figure 3, the theoretical stability boundary, which corresponds to the primary bifurcation curve, is plotted as a function of the displacement amplitude of the base, see Equation (11). The mass reaches a 25.8 mm maximum displacement at 3 Hz. The pendulum is unstable in the zone above stability boundary line. The predicted boundary is satisfactory in comparison to the experimental instability threshold. The first minimum of the curve corresponds to classical critical condition $\omega \cong 2\omega_1$ and the second one to $\omega \cong \omega_0$. The slight discrepancy observed between these two minima is due to a bad knowledge of experimental initial angular position and to a nonpure sine motion of the mass (Figure 3). In Figure 4 the theoretical and experimental stability limits are plotted as $1/\eta^2$ *versus* the displacement amplitude of the

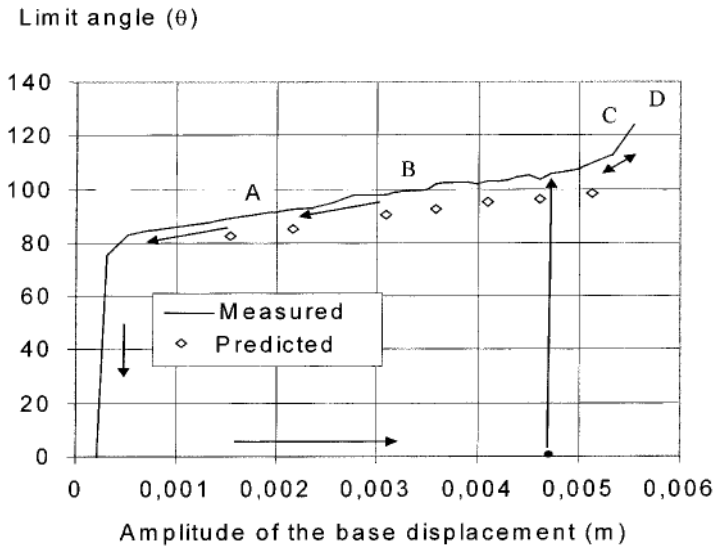

Figure 5. Bifurcation diagram.

mass M, see Equation (12). Thus the classical Strutt diagram is obtained for the first-order approximation, [13]. Here the only one minimum of the unstable region is for $\omega = 2\omega_1$.

4.2. Bifurcation Diagram

Figure 5 presents the bifurcation diagram at 3.5 Hz (thus $\eta = 1.79$, $\varepsilon = 0.072$, and $a = 4.62$ mm, see the arrow in Figure 3). The angular position limits are plotted *versus* the displacement of the base representing the amplitude of the periodic term. It is seen from the diagram that the null position of the pendulum becomes unstable at about 4.7 mm due to a period-doubling bifurcation. At this point the period 2 motion is stable and remains so until the base amplitude is decreased to a very small value where it becomes unstable and the zero equilibrium is recovered. It should be noted that the damping of the pendulum has been evaluated for small oscillations only and therefore, can affect the results. The symbolic version of the Floquet transition matrix for Equation (13) permits us to predict that the primary bifurcation takes place at 4.7 mm, which matches the numerical and measured results, see Figure 5. The motion of the pendulum is analyzed in detail at points A, B, C and D (located on Figure 5); the corresponding base displacements are 1.74, 3.37, 5.53 and 5.73 mm, respectively. Figures 6 and 7 represent motion at points A, B and C and show the predicted and measured phase-plane and Poincaré portraits. At point C it is clear that the motion is quasiperiodic. The secondary bifurcation can also be studied in symbolic form following the work of Butcher and Sinha [14]. However, it is not reported here. The disorder in the motion increases with the base displacement amplitude. The motion of the pendulum becomes chaotic above the 5.7 mm displacement amplitude and there is a sequence of successive events: revolutions clockwise or counter clockwise, stops, oscillations, etc. The computed and the measured motions of the pendulum present a similar phenomenon (see Figure 8). Beginning with oscillations around its static equilibrium position, the pendulum suddenly jumps with several entire revolutions to another equilibrium position, and so on.

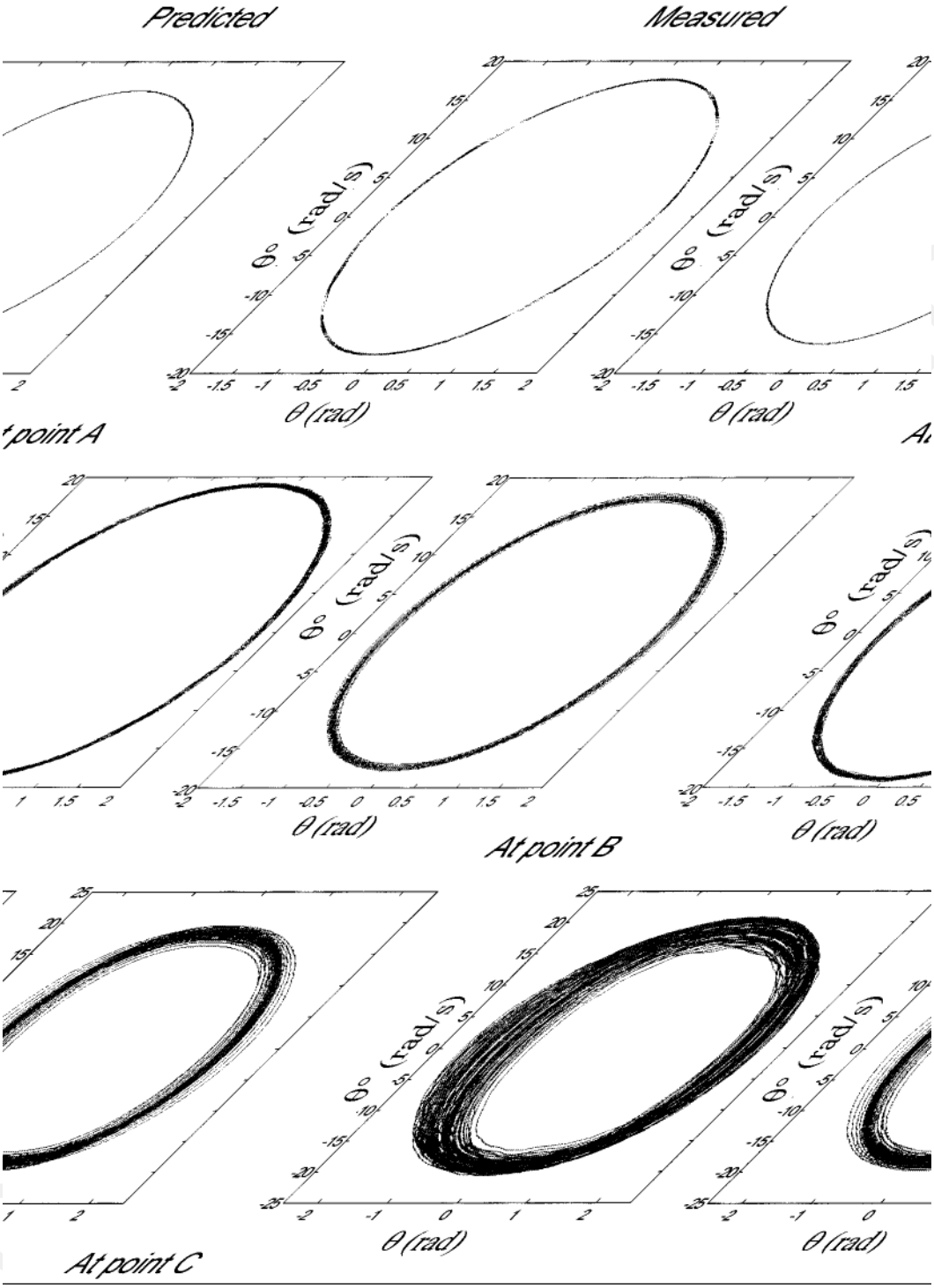

Figure 6. Predicted and measured phase-plane portraits at points A, B and C.

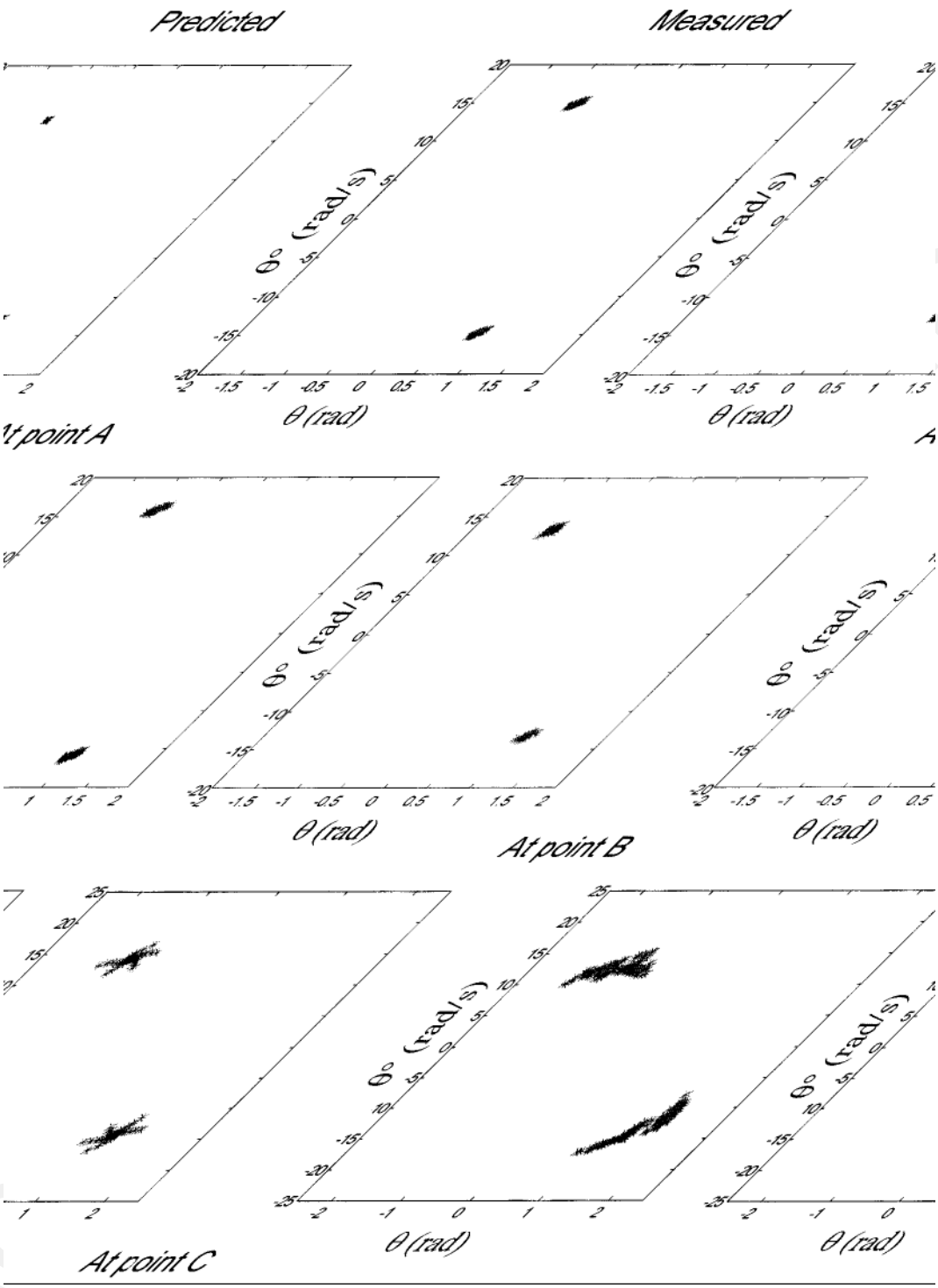

Figure 7. Predicted and measured Poincaré portraits at points A, B and C.

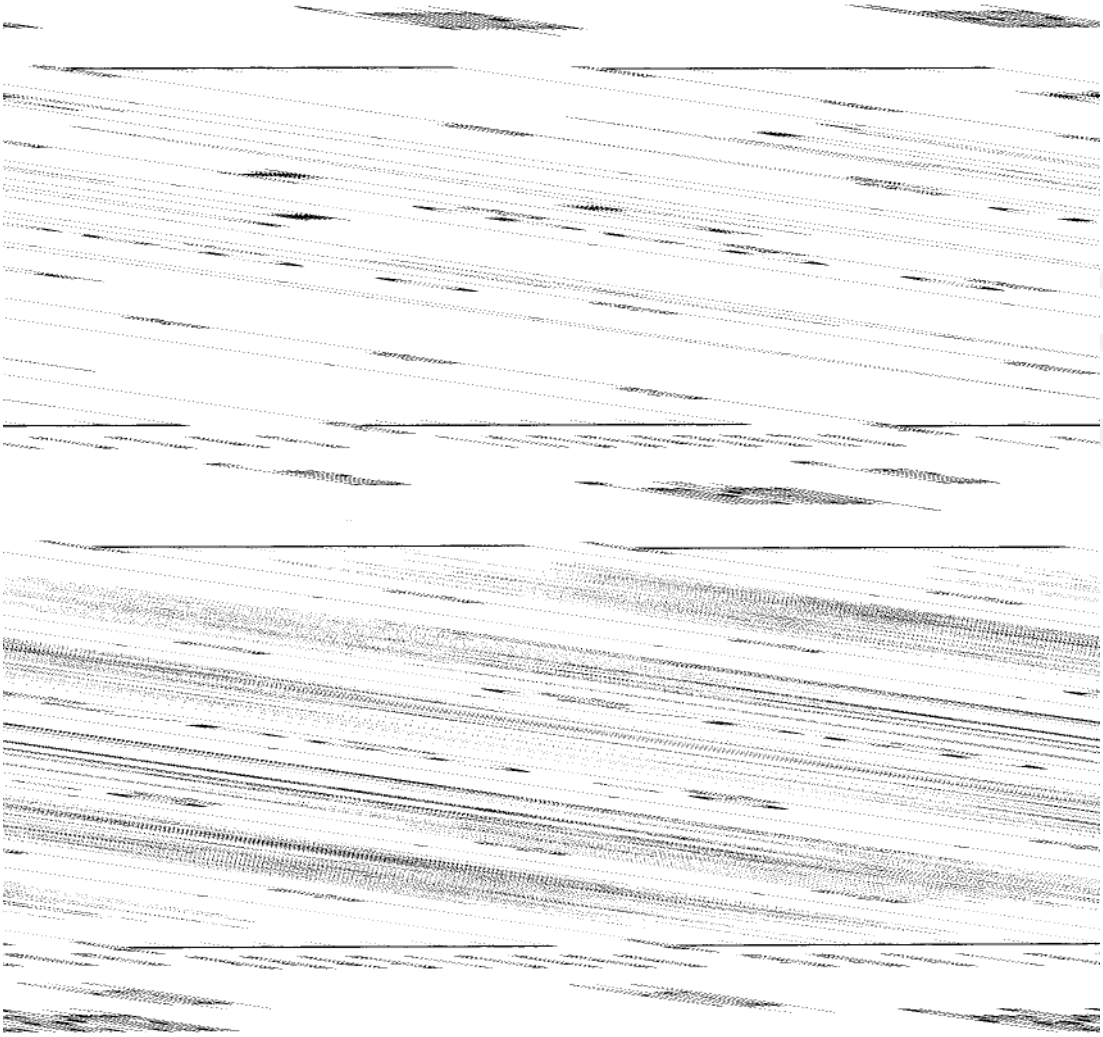

Figure 8. Computed chaotic motion of the pendulum.

5. Conclusions

In the present study, the dynamic behavior of a discrete nonlinear autoparametric system was investigated both experimentally and theoretically. The experimental set-up has permitted validation of the basic phenomena exhibited by the parametrically excited subsystem. This has been achieved using an efficient opto-electronic sensor. It has been shown that the comparison of predicted and measured results is satisfactory for the stability and bifurcation diagrams and that the motion of the pendulum becomes chaotic for relatively large base displacement amplitudes. At this state, the computed and the measured motions of the pendulum present a similar phenomenon but are not strictly identical due to the difficulty to control accurately the four experimental initial conditions of the pendulum and of mass-spring system. Further investigations will be reported on secondary bifurcations and systems with multiple degrees of freedom.

References

1. Cartmell, M., *Introduction to Linear, Parametric and Nonlinear Vibrations*, Chapman and Hall, London, 1990.
2. Nayfeh, A. H. and Mook, D. T., *Nonlinear Oscillations*, Wiley-Interscience, New York, 1979.
3. Thompson, J. M. T. and Stewart, H. B., *Nonlinear Dynamics and Chaos*, Wiley, New York, 1986.
4. Nayfeh, A. H. and Balachandran, B., *Applied Nonlinear Dynamics*, Wiley-Interscience, New York, 1995.
5. Berjé, P., Pomeau, Y., and Vidal, Ch., *L'ordre dans le chaos*, Hermann, Paris, 1995.
6. Bajaj, A. K., Chang, S. I., and Johnson, J. M., 'Amplitude modulated dynamics of a resonantly excited autoparametric two degree-of-freedom system', *Nonlinear Dynamics* **5**, 1994, 433–457.
7. Hatwal H., Mallik A. K., and Ghosh, A., 'Non-linear vibrations of harmonically excited autoparametric system', *Journal of Sound and Vibration* **81**(1), 1982, 153–164.
8. Tondl, A. and Nabergoj, R., 'Model simulation of parametric excited ship rolling', *Nonlinear Dynamics* **1**, 1990, 131–141.
9. Sinha, S. C. and Butcher, E. A., 'Symbolic computation of fundamental solution matrices for time-periodic dynamical systems', *Journal of Sound and Vibration* **206**(1), 1997, 61–85.
10. Moon, F. C., *Chaotic and Fractal Dynamics*, Wiley, New York, 1992.
11. Svoboda, R., Tondl, A., and Verhulst, F., 'Autoparametric resonance by coupling of linear and non-linear systems', *International Journal of Non-Linear Mechanics* **29**(2), 1994, 225–232.
12. Butcher, E. A. and Sinha, S. C., 'Symbolic computation of local stability and bifurcation surfaces for nonlinear time-periodic systems', *Nonlinear Dynamics* **17**, 1998, 1–21.
13. Ziegler, H., *Principles of Structural Stability*, 2nd edition, Birkhäuser, Basel, 1977.
14. Butcher E. A. and Sinha, S. C., 'Symbolic computation of secondary bifurcations in a parametrically excited pendulum', *International Journal of Bifurcation and Chaos* **8**(3), 1998, 627–637.